

# Enhancing the Mechanical Properties and Formability of Low Carbon Steel with Dual-Phase Microstructures

M. Habibi, R. Hashemi, E. Sadeghi, A. Fazaeli, A. Ghazanfari, and H. Lashini

(Submitted July 17, 2015; in revised form December 21, 2015; published online January 14, 2016)

**In the present study, a special heat treatment cycle (step quenching) was used to produce a dual-phase (DP) microstructure in low carbon steel. By producing this DP microstructure, the mechanical properties of the investigated steel such as yield stress, tensile strength, and Vickers hardness were increased 14, 55, and 38%, respectively. In order to investigate the effect of heat treatment on formability of the steel, Nakazima forming test was applied and subsequently finite element base modeling was used to predict the outcome on forming limit diagrams. The results show that the DP microstructure also has a positive effect on formability. The results of finite element simulations are in a good agreement with those obtained by the experimental test.**

**Keywords** dual-phase steel, finite element modeling, forming limit diagram, mechanical property, step quenching

## 1. Introduction

Dual-phase (DP) steels are advanced high-strength (AHS) steels, primarily comprised martensite and ferrite. Due to the good combination of strength, ductility, and formability, DP steels have been the focus of noticeable research and development efforts during the past decade (Ref 1-5). Because of the higher strength against density ratio compared to low carbon steels as well as their capability of energy absorption, DP steels have been at the center of attention in different industries such as transportation specifically automotive industry (Ref 6-10). Utilizing this type of steel in the body of cars leads to weight reduction resulting in decrease in fuel consumption.

One of the most conventional methods in producing a DP steel is heat treatment. Numerous heat treatment cycles have been employed by researchers to obtain DP steels with a variety of martensite and ferrite volume fractions and morphology (Ref 7, 11, 12). Park et al. (Ref 13) used three different heat treatments (or quenching paths), namely intercritical quenching, intermediate quenching, and step quenching (SQ), to produce DP steels with different microstructures and mechanical properties. Therefore, the heat treatment paths conspicuously influence morphology, volume fraction, and distribution of ferrite and martensite, leading to a variety of formability and mechanical properties.

M. Habibi and A. Ghazanfari, Department of Mechanical Engineering, Sharif University of Technology, Tehran, Iran; R. Hashemi, School of Mechanical Engineering, Iran University of Science and Technology, Tehran, Iran; E. Sadeghi and A. Fazaeli, Department of Material Engineering and Science, Sharif University of Technology, Tehran, Iran; and H. Lashini, Mechanic and Manufacturing Faculty, University Putra Malaysia, Serdang, Malaysia. Contact e-mails: habibi\_mech@yahoo.com, ghazanfari\_ahmad@mech.sharif.ir, rhashemi@iust.ac.ir, ramin61hashemi@yahoo.com, ehsansadeghi120@gmail.com, ab.fazaeli@gmail.com, and hadi\_1911@yahoo.com.

As mentioned, one of the most significant features of DP steel is formability (Ref 14). The forming limit analysis and the study of forming limit diagram for these types of steels have been carried out extensively by some researchers (Ref 13, 15-17). Ozturk et al. (Ref 10) investigated the formability of the AHS DP600 experimentally and numerically. They used three different anisotropic yield criteria, Hill-48, Barlat-89, and YLD2000-2d, in order to predict the FLD of the DP600 steel. Other researchers also investigated the effect of different yield criteria on prediction of FLD (Ref 18).

Although various studies have been done on DP steels, however, previous studies mainly focused only on one aspect of DP steels. They investigated DP steels mainly from the metallurgical or a mechanical point of view; however, in the present study, the authors have tried to have a comprehensive look at these types of steels. The main aim of this paper is to produce a dual-phase microstructure in a low carbon steel, which has the advantage of reduced cost, superior formability, and excellent surface finish in comparison to other high-strength low-alloy steels (Ref 1). To attain this objective, the SQ is used as a heat treatment cycle. The tensile test and micro-hardness are employed to compare the mechanical properties of the type of steel under study before and after heat treatment. The formability of steel is investigated via Nakazima forming test, and then, the FE base model is employed to predict the effect of SQ on the FLD. Finally, the forming limit predictions are compared with the experimental results and discussed later.

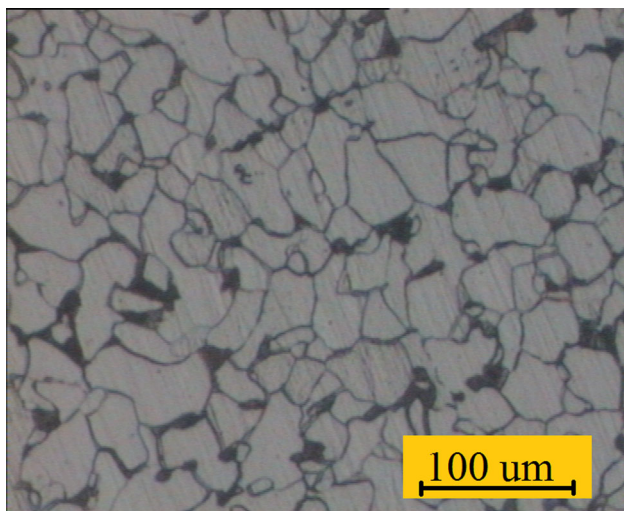
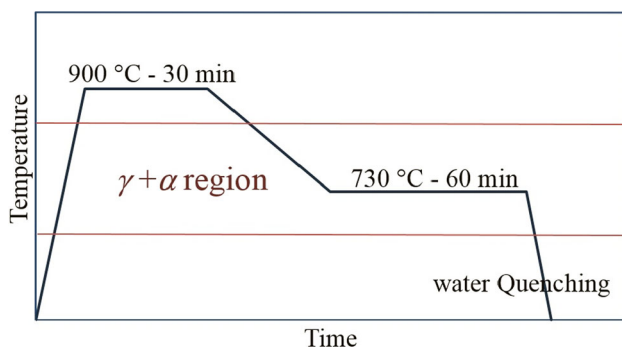
## 2. Materials and Methods

A low carbon steel sheet was used as the initial material. The chemical compositions of the investigated steel were determined using optical emission spectroscopy, and the results are shown in Table 1.  $A_{c1}$  and  $A_{c3}$  are critical temperatures, which are calculated from the empirical formula (Ref 19) given in Table 1.

The steel was first normalized in 900 °C for half an hour and cooled in air. Figure 1 indicates the ferrite-pearlite microstructure of normalized steel.

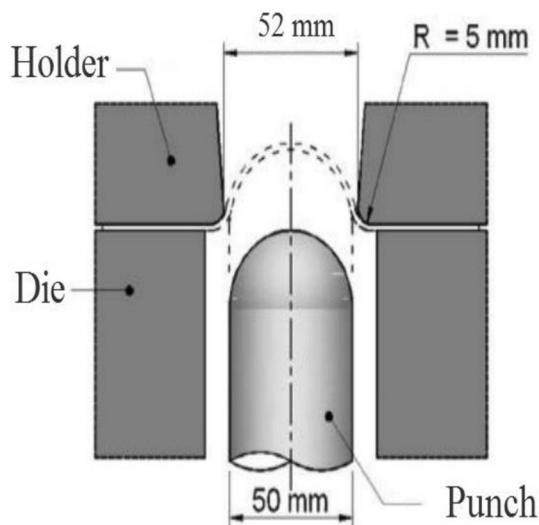
**Table 1 Chemical composition and critical temperature of the investigated steel**

Fe	C	Mn	Si	Cr	Al	Cu	Ni	Ti	P	A <sub>c1</sub>	A <sub>c3</sub>	M <sub>s</sub>
Balance	0.112	1.57	0.38	0.33	0.03	0.031	0.03	0.009	0.017	695.5 °C	859 °C	351 °C

**Fig. 1** The ferrite-pearlite microstructure of normalized steel**Fig. 2** The heat treatment (SQ) path used to produce DP microstructure

To avoid the effect of oxidation and decarbonation on the final results, dimensions of samples for heat treatment were  $110 \times 150 \times 12 \text{ mm}^3$ . After producing the DP steel, samples were cut into specimens with 2 mm thickness for mechanical tests.

The SQ process was then performed as a heat treatment process in order to obtain the DP microstructure. In this heat treatment process, the samples were first heated to 900 °C ( $\gamma$  region) for 30 min to achieve a complete austenite microstructure and then were slowly cooled to 730 °C ( $\gamma + \alpha$  region). The samples were maintained at this temperature for an hour, and eventually heat treatment process terminated with quenching the samples from 730 °C in water. The schematic of the heat treatment path is depicted in Fig. 2. The parameters of heat treatment were chosen due to the composition of low carbon steel and critical temperatures, specifically calculated for this steel (Table 1).

**Fig. 3** Schema of the Nakazima forming test

Sample preparation for the optical microscopy analysis was based on the ASTM: E3 standard (Ref 20). After polishing, the specimens were etched with a 2% nital solution in order to reveal the general microstructural observation.

Hardness tests were also carried out with a load of 30 kg being applied for the duration of 20 s as the loading time. Hardness was measured in at least five different points of each specimen, and the data were reported as Vickers hardness numbers. The tensile test specimens were prepared in sub-size dimensions based on the ASTM: E8 standard (Ref 21). Tensile tests were carried out at room temperature using an Instron tensile machine with a crosshead speed of 1 mm/min (strain rate of  $4.6 \times 10^{-4}$ /s). For further study on formability of the investigated steel, the tensile test specimens were prepared in three directions (0°, 45°, and 90°). X-ray measurements were performed on a Philips X'PERT MPD diffractometer with Cu K $\alpha$  radiation ( $K\alpha = 0.1542 \text{ nm}$ ).

To study the formability, the biaxial stretch-forming tests were carried out according to the Nakazima forming test. The schematics of the punch, lower die, and upper die are shown in Fig. 3 according to ISO 12004 standard (Ref 22). Circular grids with a 2.5 mm diameter were marked on each sample sheet by electrochemical etching. A 60 tonnes hydraulic press with a constant speed was used to draw the specimens.

To prepare the specimens for Nakazima stretching test after heat treatment, samples were prepared as shown in Fig. 4.

Finally, Nakazima forming test was simulated in 3D by using ABAQUS/Explicit software to predict the forming limit diagrams of the investigated steel before and after SQ. Hill's 1948 yield function was employed to model the behavior of the sheet metals. Holloman's Hardening law was also applied to describe work-hardening behavior.

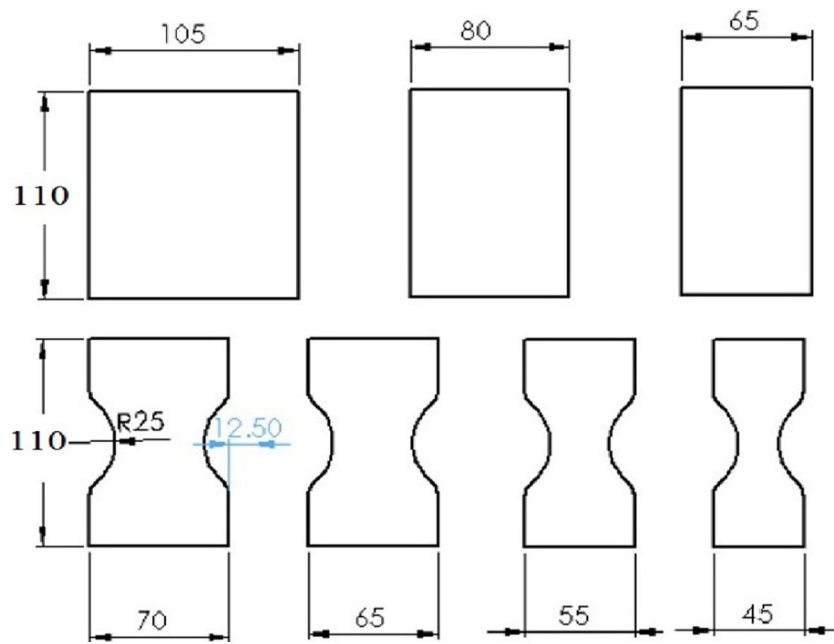


Fig. 4 Different specimens' geometry of Nakazima stretching test used in this study (all dimensions are in mm)

### 3. Results and Discussion

#### 3.1 Microstructures

Figure 5(a) shows the ferrite-martensite (DP) microstructure of steel after SQ. As mentioned earlier, before SQ, the initial steel underwent a normalizing process which leads to a ferrite-pearlite microstructure with equiaxed grains that are in equilibrium state and typical microstructure for low carbon steels (Fig. 1). During SQ, when the specimens cool from  $\gamma$  region to  $\gamma + \alpha$  region, ferrite grains are nucleated at the austenite grain boundaries and grow into the austenite. By quenching in water, the austenite is transferred to martensite and DP steel is produced. The morphology of phases consists of blocky-shaped martensite islands being distributed uniformly in coarse and equiaxed ferrite matrix (Ref 13).

The volume fraction of ferrite and martensite are graphically marked and measured by the microstructural image processor (Fig. 5b), and the result of this measurement shows the formation of 15% martensite and 85% ferrite.

Since the annealing time in 730 °C is lengthy, an equilibrium microstructure can be obtained. Based on the Lever rule in this temperature for our special low-alloy steel, the equilibrium temperature consists of about 16% austenite. Consequently, based on the sample dimensions, along with high  $M_s$  temperature in low carbon steels, deprivation of elements which stabilize austenite, and quenching samples in water, it is reasonable to assume that 15% martensite measured by the microstructural image processor is real, and thus, the idea of presence of retained austenite can be ignored.

Figure 6 shows the XRD pattern of DP microstructure. This pattern has peaks in angles like a DP600 steel (Ref 23), proving the formation of DP steel in the present study, too. As it is obvious in Fig. 6, no cementite or retained austenite peaks can be seen in a pattern, meaning that all austenite has returned to martensite.

#### 3.2 Mechanical Properties

Figure 7 shows the engineering stress-strain curve for the investigated steel with two distinct microstructures. These

curves are for tension samples with zero direction of tension. More details of given curves and the result of hardness are subsequently presented in Table 2.

As it is evident in Table 2, the mechanical properties of the investigated steel such as yield stress, tensile strength, and hardness have increased significantly after heat treatment, whereas the elongation has had an unjustifiable decrease. Moreover, it is obvious that neither in ferrite-pearlite microstructure nor in DP microstructure, the test direction has a tangible effect on yield stress or UTS. This is because of equiaxed grains and uniform distribution of pearlite and martensite in a ferrite matrix in both microstructures.

Besides all discussed mechanical improvements in DP steels, the absence of Lüder bands during plastic flow is another advantage of this type of steels, which is reported by many researchers (Ref 12, 24, 25). It is seen in Fig. 7 that in the present study these bands are also absent.

Increasing the parameters of strength coefficient ( $k$ ) and strain-hardening exponent ( $n$ ) illustrates the improvement of formability. More details on formability are provided in the following section

#### 3.3 Formability

The effect of SQ heat treatment on formability of the investigated steel was studied experimentally and numerically. The forming limit diagram determination is based on the Nakazima forming test.

**3.3.1 Experimental Results.** The FLD of the investigated steel with two different microstructures is presented in Fig. 8. To achieve these results, the samples were prepared in different dimensions (see Fig. 4). The results show that DP microstructure also has a positive effect on formability. As mentioned in Table 2, after heat treatment, the  $n$  and  $k$  parameters have increased but  $\bar{r}$  has decreased. These parameters have a direct correlation with FLD, and various investigations have been done on the effect of these parameters on FLD (Ref 26-28). To be more precise for formability investigation of the investigated steel before and after SQ, the forming limit diagram can be

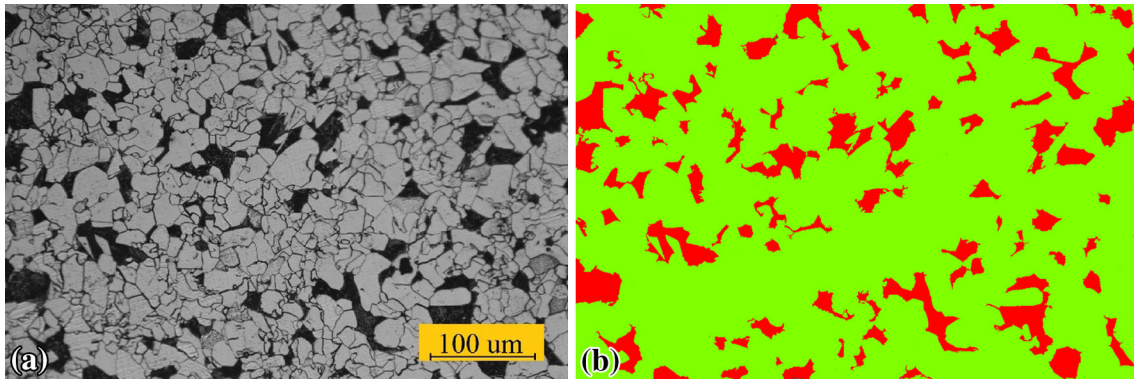


Fig. 5 (a) DP microstructure of the investigated steel. (b) The volume fraction of martensite (red objects)

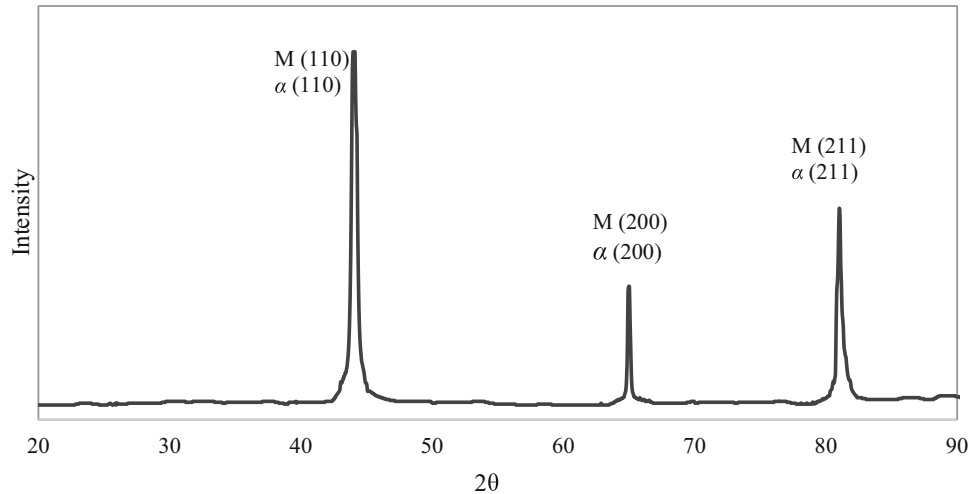


Fig. 6 XRD pattern of DP microstructure

Table 2 The mechanical property of the investigated steel for two different microstructures

	Hardness, VHN	Tension test direction	YS, MPa	UTS, MPa	% Uniform elongation	% Total elongation	$r$ value	$\bar{r}^a$	$n$	$k$ , MPa
Ferrite-perlite microstructure	127	0	360	409	22.5	34.1	0.865	0.895	0.16	443
		45	365.6	409.1	24.3	32.8	0.887			
		90	370.7	404.8	23.7	33.7	0.943			
Ferrite-martensitic microstructure	175	0	408	627.4	19.1	26.8	0.68	0.705	0.19	1083
		45	416.3	633.7	20.0	27.9	0.67			
		90	420.6	640.5	19.7	27.0	0.8			

$$^a \bar{r} = \frac{r_0 + 2r_{45} + r_{90}}{4}$$

divided into three sectors:  $FLD_0$ , the right hand side and the left hand side of the diagram. The  $FLD_0$  is influenced tangibly by the strength coefficient and strain-hardening exponent (Ref 26). Thus, as it is clear in Fig. 8, by increasing both  $k$  and  $n$  in the investigated steel after SQ, the  $FLD_0$  increases significantly. The increase in  $FLD$  after SQ is even more appreciable in the right hand side of the diagram because in this sector, in addition to the increase in  $n$  and  $k$ , the reduction of  $\bar{r}$  also has a positive effect on formability (Ref 27).

In contrast to the right hand side of the forming limit diagram, the increase in formability in the left hand side is rather lower. It is because in this sector the reduction of  $\bar{r}$  has

a negative effect on  $FLD$  (Ref 27). Figure 9 shows two samples of the investigated steel after Nakazima forming test.

**3.3.2 FE Simulation.** The Nakazima forming test was simulated using ABAQUS/Explicit to study the formability of steel before and after SQ. The friction coefficient between the blank and the punch ( $\mu$ ) was assumed to be 0.08. Die and punch were modeled as a rigid body. The blank-holder and the punch were allowed to move in the Z direction along the axis of the punch and the die was fixed (Fig. 10). The blanks were modeled as deformable solids and meshed using Solid C3D8R elements.

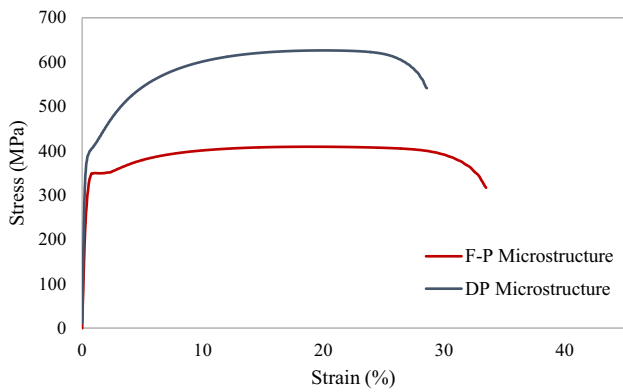


**Fig. 7** The engineering stress-strain curve for the investigated steel with two different microstructures of ferrite-pearlite (F-P) and ferrite-martensite (DP)

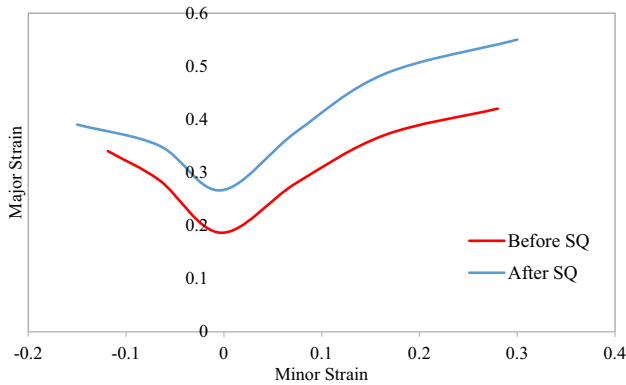


**Fig. 8** Experimentally determined FLDs of the investigated steel before and after SQ

To choose a suitable mesh size leading to accurate results without having a lengthy analysis, the mesh convergence was used. For this purpose, the force-displacement diagram of punch was utilized in one of the loading modes. Four different mesh sizes (3, 2, 1, and 0.5 mm) were deployed to consider their effects on the force-displacement diagram of punch. The results indicated that by decreasing the mesh size from 3 to 1 mm, the simulation results become more accurate. However, by decreasing the mesh size from 1 to 0.5 mm, even though as the analysis time increased, no significant improvement was observed in the accuracy of the results. Therefore, the mesh size of 1 mm was finally ratified as the suitable mesh size.

Hill's 1948 yield function was employed to model the behavior of the sheet metals. The model is described via the following relations (Ref 29):

$$f(\sigma) = \sqrt{F(\sigma_{22} - \sigma_{33})^2 + G(\sigma_{33} - \sigma_{11})^2 + H(\sigma_{11} - \sigma_{22})^2 + 2L\sigma_{23}^2 + 2M\sigma_{13}^2 + 2N\sigma_{12}^2} \quad (\text{Eq 1})$$

$$F = \frac{1}{2} \left( \frac{1}{R_{22}^2} + \frac{1}{R_{33}^2} - \frac{1}{R_{11}^2} \right) \quad (\text{Eq 2})$$

$$G = \frac{1}{2} \left( -\frac{1}{R_{22}^2} + \frac{1}{R_{33}^2} + \frac{1}{R_{11}^2} \right) \quad (\text{Eq 3})$$

$$H = \frac{1}{2} \left( \frac{1}{R_{22}^2} - \frac{1}{R_{33}^2} + \frac{1}{R_{11}^2} \right) \quad (\text{Eq 4})$$

$$L = \frac{3}{2R_{23}^2} \quad (\text{Eq 5})$$

$$M = \frac{3}{2R_{13}^2} \quad (\text{Eq 6})$$

$$N = \frac{3}{2R_{12}^2} \quad (\text{Eq 7})$$

where  $F$ ,  $G$ ,  $H$ ,  $L$ ,  $M$ , and  $N$  are Hill's yield function coefficients. These coefficients can be imported into the software by six yield stress parameters  $R_{11}$ ,  $R_{22}$ ,  $R_{33}$ ,  $R_{12}$ ,  $R_{13}$ , and  $R_{23}$ . The parameters can be computed through the anisotropic parameters  $r_0$ ,  $r_{45}$ , and  $r_{90}$  as follows (Ref 30):

$$R_{11} = R_{13} = R_{23} = 1 \quad (\text{Eq 8})$$

$$R_{22} = \sqrt{\frac{r_{90}(r_0 + 1)}{r_0(r_{90} + 1)}} \quad (\text{Eq 9})$$

$$R_{33} = \sqrt{\frac{r_{90}(r_0 + 1)}{(r_{90} + r_0)}} \quad (\text{Eq 10})$$

$$R_{12} = \sqrt{\frac{3(r_0 + 1)r_{90}}{(2r_{45} + 1)(r_{90} + r_0)}} \quad (\text{Eq 11})$$

Holloman's hardening law was used to describe work-hardening. The law is given in the following equation:

$$\bar{\sigma}_Y = K(\bar{\epsilon})^n \quad (\text{Eq 12})$$

where  $\bar{\sigma}_Y$  denotes the effective stress,  $\bar{\epsilon}$  is the effective strain,  $n$  is the strain-hardening exponent, and  $K$  is the strength coefficient. By extracting strain-hardening exponent ( $n$ ) and the strength coefficient ( $k$ ) from stress-strain curves and using Holloman equation (Eq 12), the strain-hardening behavior of material was imposed to FE software.

Due to a fast local change of sheet thickness in the necking point, the thickness strain leaping changes its value. The necking criteria are the second-time derivative of the thickness strain (SDT) given by the following equation (Ref 31, 32):

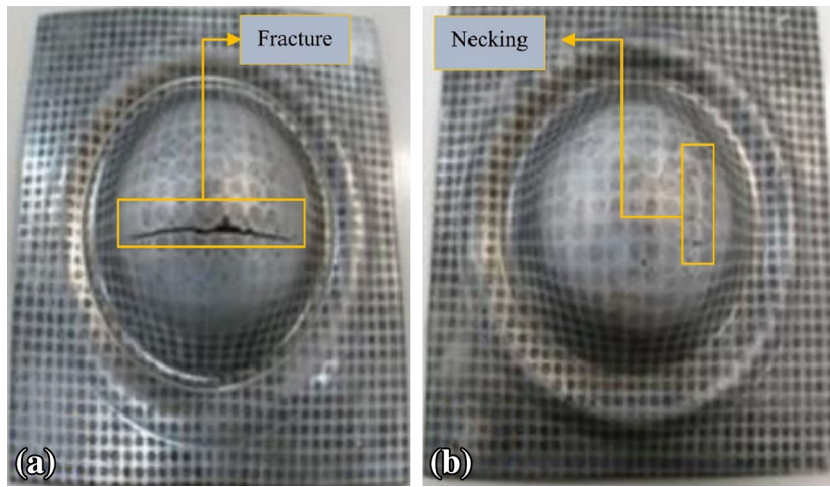


**Fig. 9** The formed samples after failure in Nakazima forming test for the investigated steel: (a) before SQ and (b) after SQ

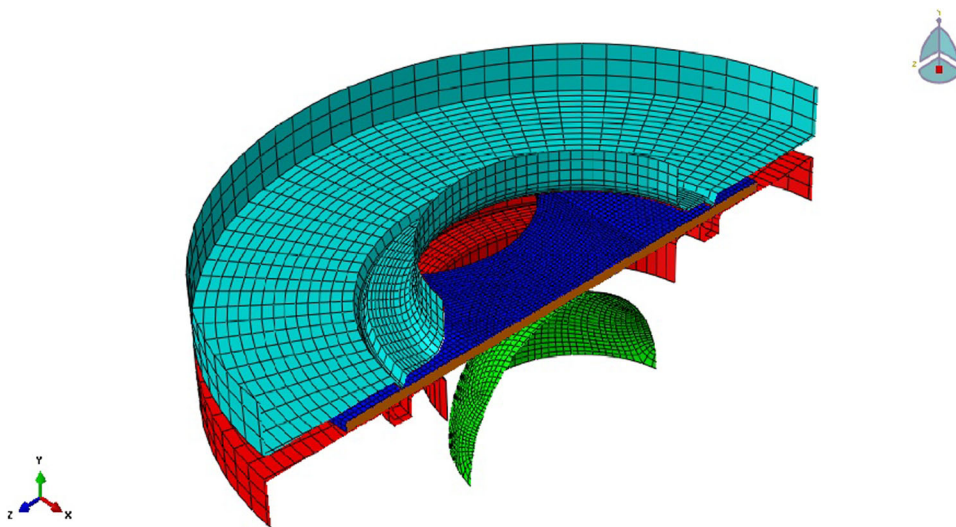


**Fig. 10** Typical view of the 3D model including the punch, the blank-holder, the sheet, and the die

$$\ddot{\epsilon}_{33} = \frac{(d^2 \epsilon_{33})}{(dt^2)} \quad (\text{Eq 13})$$

where  $\epsilon_{33}$  is the thickness strain of the element. The element where the peak of  $\ddot{\epsilon}_{33}$  first appears (at minimal time) was assumed to be the element where the onset of necking started, and the time of this peak was considered the necking time. The following steps should be taken to achieve necking time:

1. Extracting the diagram of thickness strain versus time (Fig. 11a)
2. Calculating the second derivative of the diagram obtained in step 1 (Fig. 11c).
3. Considering the time when the curve obtained in step 2 is extremum as the necking time.

The FLDs for the investigated steel sheet before and after SQ simulated by FE model are presented in Fig. 12.

As it is clear from Fig. 12, the results of FE modeling are in a good agreement with the experimental results. One of the

reasons for the accuracy of this model is using Solid C3D8R elements for meshing, which imposes whole stress tensor components in FE analysis (Ref 30-34). Due to the great influence of mesh size on the accuracy of results, a variety of mesh sizes have been tested to reach the most accurate results. Finally, the mesh size of 1 mm was ratified as the most accurate result. A minor deviation in the curve is due to this assumption in modeling that the material is assumed to be isotropic while in reality it is not (see Table 2).

## 4. Conclusions

The DP microstructure was successfully produced in low carbon steel by Step Quenching. The morphology of the phases consists of large blocky martensite islands with 15% volume fraction uniformly distributed in the coarse ferrite matrix. By producing this DP microstructure, the mechanical properties of the investigated steel such as yield stress, tensile strength, and Vickers hardness have increased 14, 55, and 38%, respectively.

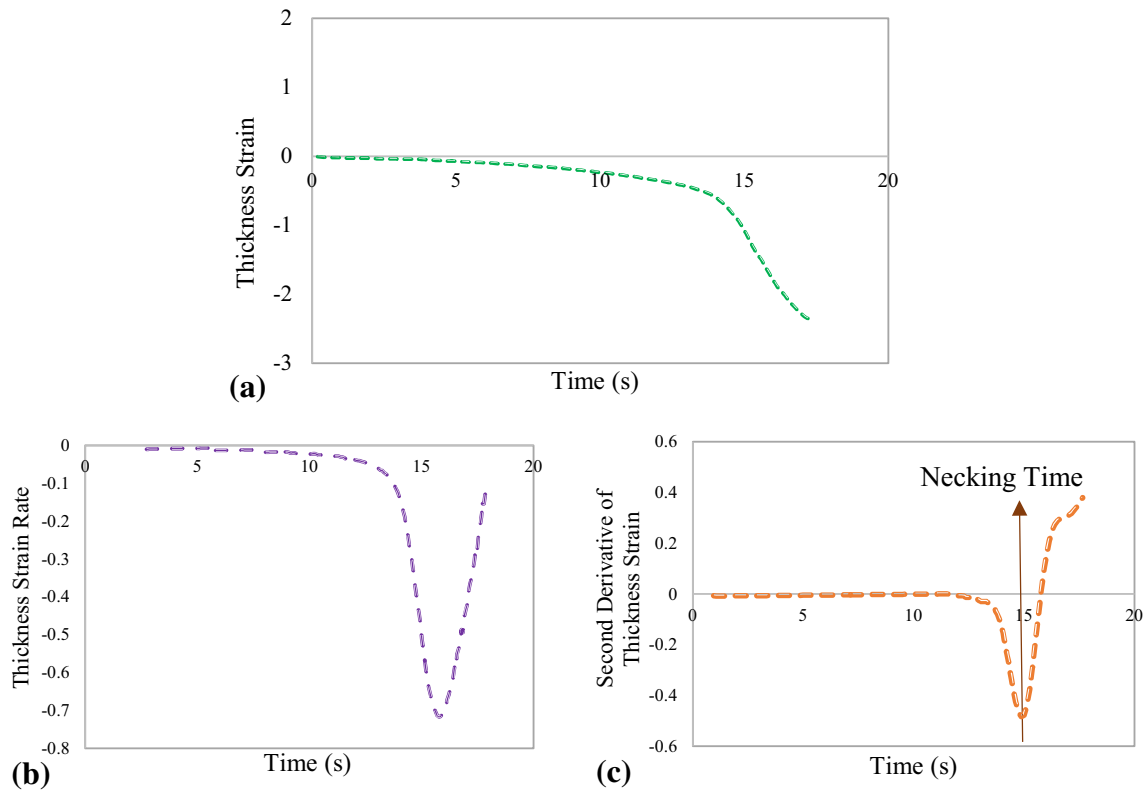


**Fig. 11** Procedure for extracting sheet metal forming strains in FE simulation

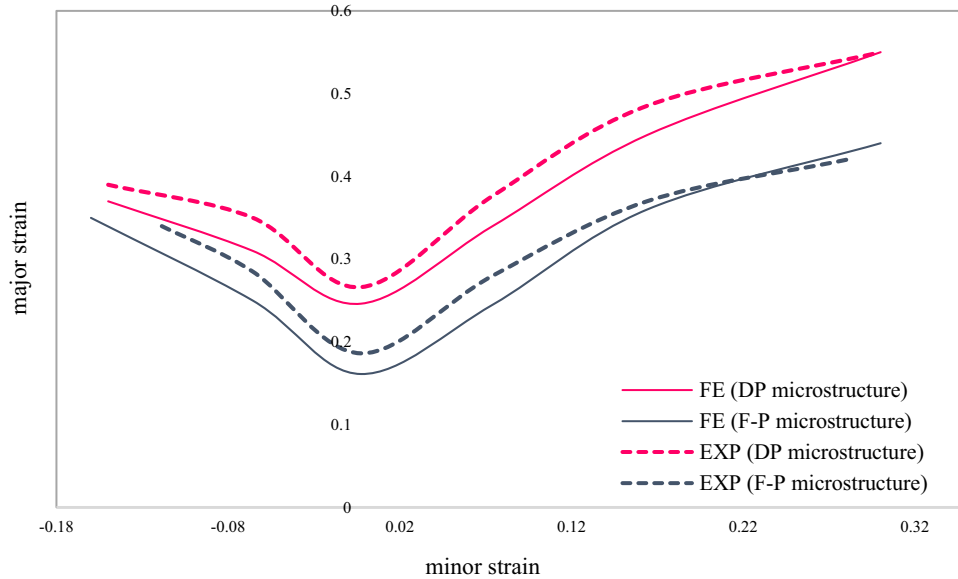


**Fig. 12** The experimental and numerical FLDs of the investigated steel before and after SQ

The absence of Luder bands was another positive result of producing DP microstructure. The formability of steel sheets with Nakazima forming test approach was determined experimentally and numerically before and after SQ. The results of the experimental study illustrate a significant increase in FLD of the low carbon steel with DP microstructure in comparison to that of ferrite-pearlite. Formability in all areas of the FLD

(FLD<sub>0</sub>, the right hand side and the left hand side) has increased owing to the enhancement of strength coefficient and strain-hardening exponent and the reduction of  $\bar{r}$ . For a numerical study on formability, Nakazima forming test was simulated in 3D using ABAQUS/Explicit software. The results of the simulation were in a good agreement with those of the experimental tests.

## References

1. F.M. Al-Abbasi and J.A. Nemes, Micromechanical Modeling of Dual Phase Steels, *Int. J. Mech. Sci.*, 2003, **45**, p 1449–1465
2. S.K. Paul, Effect of Martensite Volume Fraction on Stress Triaxiality and Deformation Behavior of Dual Phase Steel, *Mater. Des.*, 2013, **59**, p 782–789
3. S. Kuang, Y. Kang, H. Yu, and R. Liu, Stress-Strain Partitioning Analysis of Constituent Phases in Dual Phase Steel Based on the Modified Law of Mixture, *Int. J. Miner. Metall. Mater.*, 2009, **16**, p 393–398
4. H. Xu, W. Yang, and Z. Sun, Mechanical Properties of Fine-Grained Dual Phase Low-Carbon Steels Based on Dynamic Transformation, *J. Univ. Sci. Technol. Beijing*, 2008, **15**, p 556–560
5. C.F. Kuang, J. Li, S.G. Zhang, J. Wang, H.F. Liu, and A.A. Volinsky, Effects of Quenching and Tempering on the Microstructure and Bake Hardening Behavior of Ferrite and Dual Phase Steels, *Mater. Sci. Eng., A*, 2014, **613**, p 178–183
6. M.J. Molaei and A. Ekrami, The Effect of Dynamic Strain Aging on Fatigue Properties of Dual Phase Steels with Different Martensite Morphology, *Mater. Sci. Eng., A*, 2009, **527**, p 235–238
7. A. Bayram, A. Uguz, and M. Ula, Effects of Microstructure and Notches on the Mechanical Properties of Dual-Phase Steels, *Mater. Charact.*, 1999, **43**, p 259–269
8. G. Rosenberg, I. Sinaiová, and Ľ. Juhar, Effect of Microstructure on Mechanical Properties of Dual Phase Steels in the Presence of Stress Concentrators, *Mater. Sci. Eng., A*, 2013, **582**, p 347–358
9. S. Sodjit and V. Uthaisanguk, Microstructure Based Prediction of Strain Hardening Behavior of Dual Phase Steels, *Mater. Des.*, 2012, **41**, p 370–379
10. F. Ozturka, S. Torosb, and S. Kilic, Effects of Anisotropic Yield Functions on Prediction of Forming Limit Diagrams of DP600 Advanced High Strength Steel, *Proced. Eng.*, 2014, **81**, p 760–765
11. M.R. Akbarpour and A. Ekrami, Effect of Ferrite Volume Fraction on Work Hardenin Behavior of High Bainite Dual Phase (DP) Steels, *Mater. Sci. Eng., A*, 2008, **447**, p 306–310
12. N. Saeidi and A. Ekrami, Comparison of Mechanical Properties of Martensite/Ferrite and Bainite/Ferrite Dual Phase 4340 Steels, *Mater. Sci. Eng., A*, 2009, **523**, p 125–129
13. K.S. Park, K. Park, D.L. Lee, and C.S. Lee, Effect of Heat Treatment Path on the Cold Formability of Drawn Dual-Phase Steels, *Mater. Sci. Eng., A*, 2007, **449**, p 1135–1138
14. H. Farnoush, D.H. Fatmehsari, and A. Ekrami, The Effect of Pre-straining at Intermediate Temperatures on the Mechanical Behavior of High-Bainite Dual Phase (HBDP) Steels, *Mater. Sci. Eng., A*, 2012, **543**, p 224–230
15. S.B. Kim, H. Huh, H.H. Bok, and M.B. Moon, Forming Limit Diagram of Auto-Body Steel Sheets for High-Speed Sheet Metal Forming, *J. Mater. Process. Technol.*, 2011, **211**, p 851–862
16. M. Firat, A Finite Element Modeling and Prediction of Stamping Formability of a Dual-Phase Steel in Cup Drawing, *Mater. Des.*, 2012, **34**, p 32–39
17. W. Bleck, Z. Deng, K. Papamantell, and C.O. Gusek, A Comparative Study of the Forming-Limit Diagram Models for Sheet Steels, *J. Mater. Process. Technol.*, 1998, **83**, p 223–230
18. S. Panich, F. Barlat, V. Uthaisa, and S. Suranuntchai, Experimental and Theoretical Formability Analysis Using Strain and Stress Based Forming Limit Diagram for Advanced High Strength Steels, *Mater. Des.*, 2013, **51**, p 756–766
19. G. Krauss, Steels, Heat Treatment and Processing Principles, ASM, 1990
20. <http://www.astm.org/Standards/E3.htm>
21. <http://www.astm.org/Standards/E8.htm>
22. [http://www.iso.org/iso/catalogue\\_detail.htm?csnumber=43621](http://www.iso.org/iso/catalogue_detail.htm?csnumber=43621)
23. M. Hadianfard, Low Cycle Fatigue Behavior and Failure Mechanism of a Dual-Phase Steel, *Mater. Sci. Eng., A*, 2009, **499**, p 493–499
24. A. Ghaehri, A. Shafyei, and M. Honarmand, Effects of Inter-Critical Temperatures on Martensite Morphology, Volume Fraction and Mechanical Properties of Dual-Phase Steels Obtained from Direct and Continuous Annealing Cycles, *Mater. Des.*, 2014, **62**, p 305–319
25. A.-P. Pierman, O. Bouaziz, T. Pardoën, and P.J. Jacqu, The Influence of Microstructure and Composition on the Plastic Behaviour of Dual-Phase Steels, *Acta Mater.*, 2014, **73**, p 298–311
26. A.K. Ghosh, The Influence of Strain Hardening and Strain-Rate Sensitivity on Sheet Metal Forming, *J. Eng. Mater. Technol.*, 1977, **99**, p 264–274
27. K.W. Neale and E. Chater, Limit Strain Predictions for Strain-Rate Sensitive Anisotropic Sheets, *Int. J. Mech. Sci.*, 1980, **22**, p 563–574
28. A. Graf and W.F. Hosford, Calculations of Forming Limit Diagrams, *Metall. Trans. A*, 1990, **21**, p 87–94
29. R. Hill, A Theory of the Yielding and Plastic Flow of Anisotropic Metals, *Proceedings of the Royal Society of London. Series A, Mathematical and Physical Sciences*, 1948, p 281–297
30. Abaqus User Guide, ABAQUS Analysis User's Manual
31. R.S. Korouyeh, H.M. Naeini, and G. Liaghat, Forming Limit Diagram Prediction Of Tailor-Welded Blank Using Experimental and Numerical Methods, *J. Mater. Eng. Perform.*, 2012, **21**, p 2053–2061
32. H. Mamusi, A. Masoumi, R. Hashemi, and R. Mahdavinejad, A Novel Approach to the Determination of Forming Limit Diagrams for Tailor-Welded Blanks, *J. Mater. Eng. Perform.*, 2013, **22**, p 3210–3221
33. A. Assempour, R. Hashemi, K. Abrinia, M. Ganjiani, and E. Masoumi, A Methodology for Prediction of Forming Limit Stress Diagrams Considering the Strain Path Effect, *Comput. Mater. Sci.*, 2009, **42**, p 195–204
34. E. Karajibani, R. Hashemi, M. Sedighi, Determination of Forming Limit Curve in Two-Layer Metallic Sheets Using the Finite Element Simulation, *Proceedings of the Institution of Mechanical Engineers, Part L: Journal of Materials: Design and Applications*, 2015, 1464420715593565